Sheffield Hallam University

Composition and dynamics of high power impulse magnetron discharge at W-Mo-C target in argon atmosphere

GAJEWSKI, W., EHIASARIAN, A.P. <http://orcid.org/0000-0001-6080-3946>, ŻELECHOWSKI, M. and HOVSEPIAN, P. Eh. <http://orcid.org/0000-0002-1047-0407>

Composition and dynamics of high power impulse magnetron discharge at W-Mo-C target in argon atmosphere

W. Gajewski[a)], A.P. Ehiasarian[b)], M. Żelechowski[a)], P.Eh. Hovsepian[b)]

[a)] *TRUMPF Huettinger Sp. z o.o., Marecka 47, 05-220 Zielonka, Poland*
[b)] *Materials and Engineering Research Institute, Sheffield Hallam University, Howard Street, Sheffield S1 1WB, UK*

Abstract

Metal-doped diamond-like carbon (Me-DLC) is a typical industrial solution for wear resistant coating due to their tribological properties. DLC doping with metal is used to reduce internal stress of the DLC coating, improve its thermal stability, hardness, coating-substrate adhesion, and wear resistance. Furthermore, application of the High Power Impulse Magnetron Sputtering (HiPIMS) for Me-DLC deposition allows improvement of coating adhesion and densification of the coating. To improve the properties of the DLC coatings doping with tungsten and molybdenum from a mixed W-Mo-C target can be used. This study concerns the plasma chemistry and composition for a W-Mo-C target operated with HIPIMS in argon atmosphere. For a HIPIMS discharge with a fixed pulse length of 150 μs a linear dependence of the average power and current are observed. The optical emission spectroscopy experiments reveal a temporal dependence of the plasma composition as the current pulse develops. First plasma is dominated by argon neutrals and ions followed by molybdenum and tungsten. Significant separation between the two metal species is observed in terms of the times of onset and peak of the emission. As a consequence of the change of the neutral gas to metal ratio the estimated effective electron temperature, T_e, changes from ~2 eV as estimated from Ar I emission to ~0.3-0.6 eV as indicated by W I emission. A change of T_e is also observed with the change of HIPIMS frequency: the T_e estimated from metal excitations increases most probably as a result of the processes taking place in the afterglow phase between HIPIMS pulses. The transition from argon plasma at the beginning of the pulse to metal-rich plasma in the second phase of the pulse is discussed in comparison with the ion current measurements performed with a planar probe.

1. Introduction

Metal-doped diamond-like carbon (Me-DLC) coatings can possess high hardness, low coefficients of friction against materials such as steel, and are generally chemically inert [1, 2, 3]. These desirable tribological properties arise as the properties of the film can be manipulated to give either diamond-like or graphite-like properties by controlling the deposition process. Additionally, the incorporation of nitrogen, hydrogen, silicon or metal-doping gives further possibilities of controlling the chemistry, and thus the tribochemistry of the films.

Recent study of *Mandal et al.* confirmed that a mixed Mo and W doping of DLC layer improves the tribological performance and thermal stability of the Mo-W-C coating [2]. The authors have used a mixed HIPIMS + unbalanced magnetron (UBM) sputtering technique, where one Mo-W-C target was operated with HIPIMS power supply and three graphite

targets were used in DC mode. The structural and tribological tests performed on Mo-W-C coating deposited on high speed steel (HSS) and stainless steel (SS) samples revealed a low friction coefficient ~0.335 in dry sliding as a result of the formation of a transfer layer composed of fine graphite particles and different Mo sulphates and oxides acting as solid lubricants [2].

To our knowledge there is no data in the literature on the plasma properties from the mixed Mo-W-C target operated with HIPIMS. Thus in this study properties of the plasma chemistry and ion flux generated using HIPIMS + UBM on Mo-W-C and graphite targets is investigated by means of optical emission spectroscopy (OES) and planar Langmuir probe measurements and correlated with the output current and voltage delivered by the power supply to drive the electrical discharge.

2. Experimental details

The Mo-W-C plasma was investigated in an industrial sized Hauzer HTC1000-4 PVD coating machine equipped with four planar cathodes each of target area of 1200 cm^2. Three graphite targets were operated in DC mode by Hauzer DC power supplies (maximum power of 20 kW at 750 V) and a compound target containing both Mo and W was powered with TruPlasma Hipulse HMP 2/4 power supply (maximum voltage 2 kV and maximum peak current of 4 kA). The experiments were carried out in pure Ar at working gas pressure of $3.2x10^{-3}$ mbar. The Ar flow rate was kept constant at 254 sccm. The graphite targets were operated with 5 kW each in all experiments whereas the average HIPIMS power was varied from 2.5 to 8.5 kW by the change of HIPIMS pulsing frequency. Thus, a broad range of the process parameters used in the work of *Mandal et al.* [2] have been covered. A detailed description of sample preparation, target and surface pre-treatment for coating deposition can be found in Ref. [2]. Waveforms of the cathode voltage, U_C, and of the cathode current, I_C, were measured by a Tektronix P2220 voltage probe and a Fluke i1000s current monitor, respectively, and recorded by a Tektronix DPO 7054 digital oscilloscope.

Plasma composition analysis was carried out by Jobin Yvon Triax 320 spectrometer with grating groove density of 1200 grooves/mm and quartz optical fiber and collimator in vacuum. The collimator was placed in the centre part of the vacuum chamber and it is collecting the light in direction parallel to the target. For the time-resolved optical emission measurements from the discharge the line of sight of the optical fiber was directed to be viewing the surface of the Mo-W-C target surface. During the time-averaged optical emission measurements, the spectra were recorded with a detector integration time of 2 s and averaged 5 times..

The ion saturation current measurements were performed with a flat electrostatic probe with a diameter of 2 cm equipped with a guard ring and positioned 20 cm from the target surface. The probe was biased to a negative voltage of 100 V to repel the entirety of electron flux and the ion saturation current was measured with a Tektronix P6021 current probe connected to the Tektronix DPO 7054 digital oscilloscope.

3. Results and discussion
3.1. Plasma discharge
The time dependence of the voltage and current output in the HIPIMS discharge is depicted in Figure 1. In this study pulsing frequency ranging from 48 to 200 Hz was used to control the average power delivered.
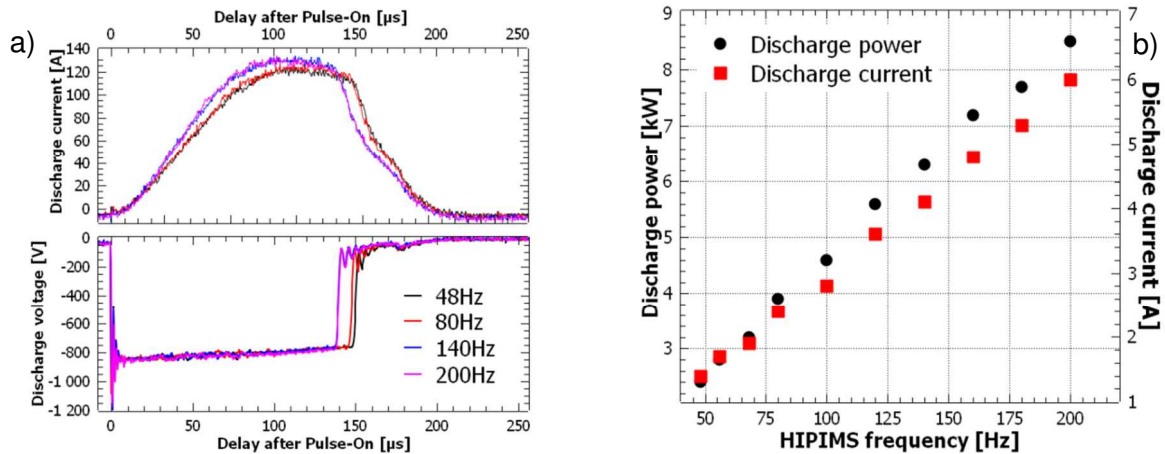
Figure 1. The voltage and current output shape as a function of HIPIMS frequency (a). In b) the dependence of the discharge average power and average current on HIPIMS frequency are shown. A pulse length of 150 µs was used for a discharge on Mo-W-C target in Ar pressure p_{Ar} = 3.2x10^{-3} mbar.

As shown in Figure 1a) the shape of the voltage and current pulse are similar for all used pulsing frequencies, except for a slight steepening of the current rise and a 10 µs shortening of the pulse length observed with the increase of the pulse frequency. Despite these differences operation in the voltage controlled mode results in a linear dependence of the average power and current on the frequency as depicted in Figure 1b). As in the case of other reports on HIPIMS discharges [4, 5], high voltage oscillations are present at the beginning of the pulse, after which the voltage slowly decreases. The onset of the current pulse follows almost immediately after the beginning of the voltage pulse indicating a small "statistical lag time" for the given voltage and gas pressure conditions. Furthermore, after reaching its maximum in 100 – 110 µs the current starts to decrease until the end of the pulse. As soon as the voltage is turned off, a steep decrease of the target current can be observed as depicted in Figure 1a).

Since in the case of HIPIMS discharges the decrease of the current was assigned to the transition between the Ar rich plasma at the beginning of the pulse to the metal rich plasma in the second part of the pulse [6], OES and planar Langmuir probe measurements have been used to compare the current understanding of the HIPIMS discharge to operation with Mo-W-C as a target material.

3.2. Plasma composition

In Figure **2** the optical emission spectra in the range of 290 – 860 nm are shown. As the graph reveals, the spectra can be divided into two parts: in the wavelength range above 650 nm intense Ar lines dominate the spectra. Below 650 nm metal lines from the target material can be resolved. Since the Mo and W ion lines are located between 180 and 210 nm which is below the spectral range of used OES setup a lower intensity of metal lines compared to the Ar dominated part of the spectra is observed. On the contrary, the position of argon ion lines is overlapping the position of Mo and W neutrals lines preventing their unequivocal identification. Furthermore, no carbon lines were identified in the spectra suggesting it to be below the detection limit.

To our knowledge this is the first report on the Ar plasma from a Mo-W-C target operated in the HIPIMS mode, thus a great attention has been given to identification of metal lines. Table 1 and Figure 3 give the summary of the metal lines wavelength and assignment. Note,

that the spectrum was collected with the collimator positioned in the center part of the vacuum chamber, thus reflecting the gas composition "seen" by the sample to be coated.
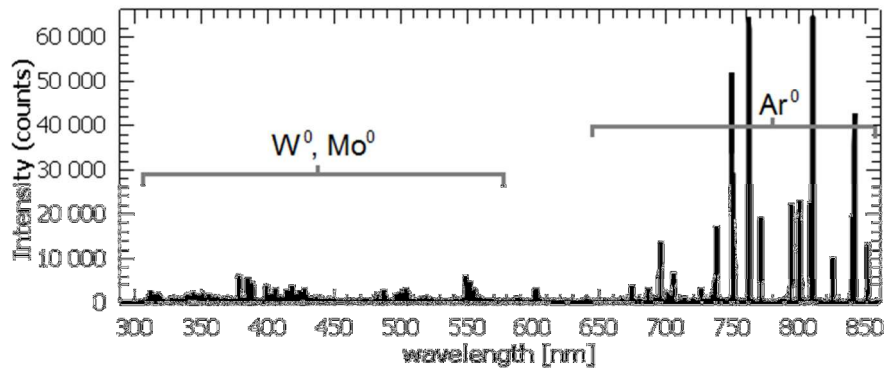

Figure 2. Optical emission spectrum of high power impulse sputtering of Mo-W-C in an argon atmosphere at f=200Hz, p_{Ar} = 3.2x10^{-3} mbar.

As can be seen in Figure 3 both W and Mo lines can be identified. Due to the difference in the transition strength the Mo lines have, however, relatively higher intensity compared to the W lines.
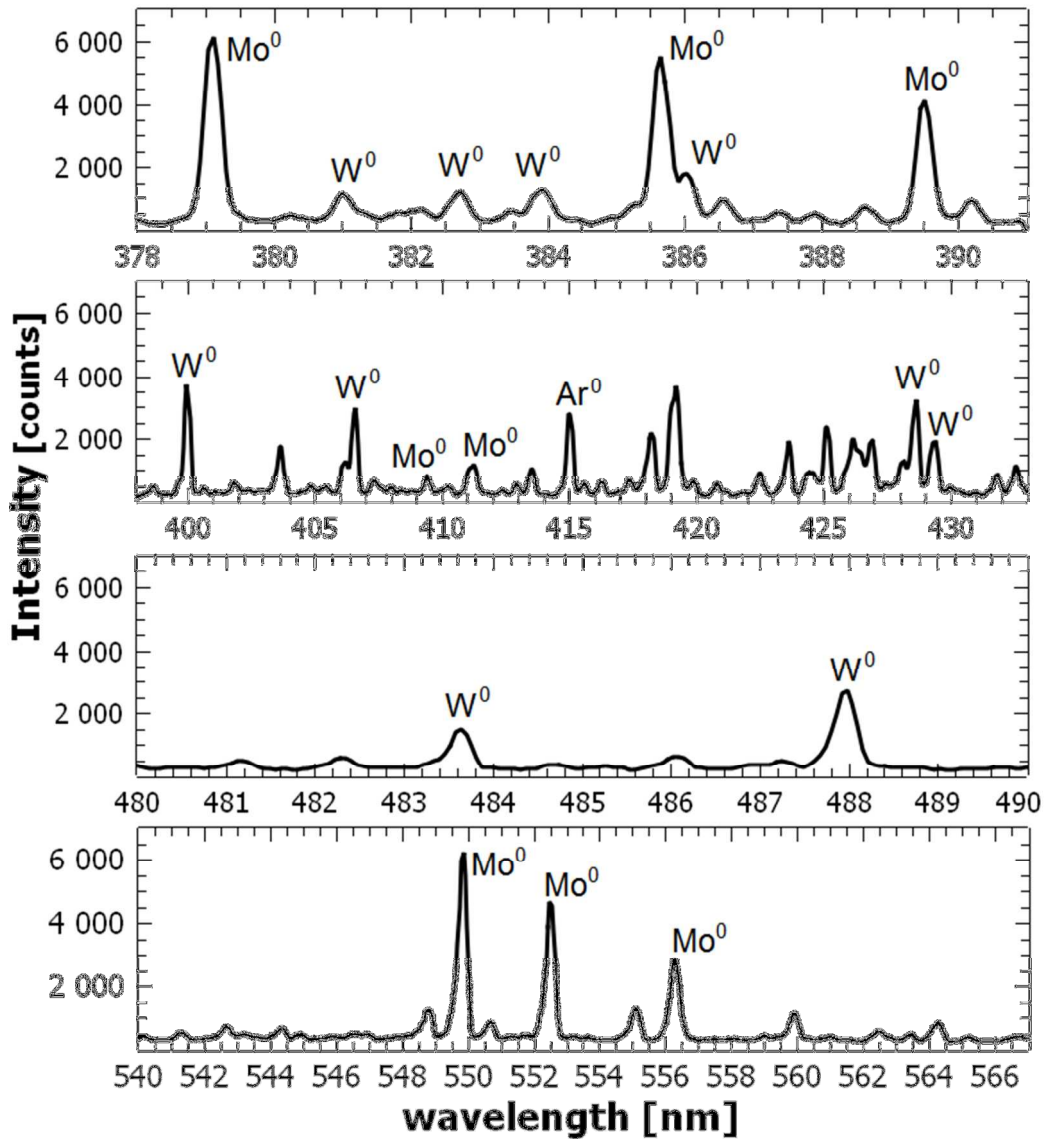
Figure 3. Identification of dominant optical emission lines from the Mo-W-C sputtering target operated in Ar atmosphere with f = 200 Hz, p_{Ar} = 3.2x10^{-3} mbar.

The metal lines have been further used to estimate the effective electron temperature of the plasma. For this, the pair-line method has been used [7]. Within this method the determination of temperature is based on the intensity ratio of two transitions of an atom between one lower energy level and two distinct upper energy levels.

Table 1. Summary of the dominant optical emission lines from Mo-W-C target operated in argon atmosphere. The wavelength (λ), the transition strength (A_{ij}) and the energy of lower (E_i) and upper (E_j) transition levels are from the NIST Atomic Spectra Database Lines Data.

Line	λ [nm]	A_{ji} ($\times10^{8}$ s^{-1})	Transition	E_i [eV]	E_j [eV]
Ar^0	415.859	0.014	4s 2<2>* -> 5p 2<2>	11.55	14.53
Ar^0	425.936	0.039	4s 1<1>* -> 5p 1<1>	11.83	14.74
Ar^0	750.387	0.445	4s 1<1>* -> 4p 1<1>	11.83	13.48
Ar^0	751.465	0.402	4s 2<2>* -> 4p 2<1>	11.62	13.27
Ar^0	852.144	0.139	4s 1<1>* -> 4p 1<2>	11.83	13.28
W^0	381.748	0.031	6s 7S -> 6s6p 5F*	0.37	3.61
W^0	384.621	0.021	6s2 5D -> 6s6p 5F*	0.21	3.43
W^0	400.875	0.163	6s 7S -> 6s6p 7P*	0.37	3.46
W^0	488.691	0.010	6s2 5D -> 6s6p 7F*	0.77	3.31
Mo^0	379.825	0.690	a7S -> z7P*	0.00	3.26
Mo^0	386.410	0.624	a7S -> z7P*	0.00	3.21
Mo^0	390.295	0.617	a7S -> z7P*	0.00	3.18
Mo^0	550.649	0.361	a5S -> z5P*	1.34	3.59
Mo^0	553.303	0.372	a5S -> z5P*	1.34	3.58
Mo^0	557.044	0.330	a5S -> z5P*	1.34	3.56

Based on the slow rise times of the current and therefore slow increase in plasma density, we can assume that the plasma is in equilibrium through most of the pulse apart from short periods at the moments of application and switch off of the voltage. The low effective electron temperatures of 2 eV detected even at long distances from the target where plasma density is lower indicate a high intensity of collisions bringing the plasma close to a local thermal equilibrium [8]. The theoretical intensity of an emission line can be expressed as: $I_{mn} = hcN_mA_{mn}/\lambda_{mn}$, and the density of lower and upper energy states can be described with Boltzmann statistics [7]. Thus, the intensity ratio of two transitions can be given as:

$$\ln\left(\frac{I_{mn}g_pA_{pn}\lambda_{mn}}{I_{pn}g_mA_{mn}\lambda_{pn}}\right) = -\frac{E_m-E_p}{kT_e} \tag{1}$$

where λ_{mn} is the wavelength and I_{mn} is the radiant intensity of the light emitted due to transition from energy level n to m, g_m is the statistical weight of energy level m, E_m is the excitation energy at energy level m, and A_{mn} is the transition probability from energy level n to m and k is the Boltzmann constant. By analogy similar notation has been used to the parameters for transition from level n to p. It is also assumed that the energy of level p is greater than the energy of level m. The intensity I_{mn} and I_{pn} from measured spectra were used and the other parameters have been obtained from the National Institute of Standards and Technology (NIST) database [9] as summarized in

Table **1**. Since this method uses relative values calibration of the absolute spectral sensitivity of the optical arrangement is not necessary which makes the application of this approach simple

The transitions used for assessment of the effective electron temperature according to Eq. (1) are summarized in

Table **2**.

Table 2. Parameters of optical emission lines used in T_e calculation with intensity ratio method. The wavelength (λ), the transition strength (A_{ij}), the statistical weight of lower and upper energy level (g_{ij}), the energy and configuration of lower (E_i) and upper (E_j) transition levels are from the NIST Atomic Spectra Database Lines Data.

Line	λ [nm]	A_{ji} (x10^8 s^{-1})	g_{ij}	E_i config.	E_i [eV]	E_j config.	E_j [eV]	dE [eV]
Ar^0	425.936	0.039	3 - 1	4s 1<1>*	11.83	5p 1<1>	14.74	2.91
Ar^0	451.073	0.012	3 - 1	4s 1<1>*	11.83	5p 2<1>	14.58	2.75
W^0	381.748	0.031	7 - 7	6s 7S	0.37	6s6p 5F*	3.61	3.25
W^0	400.875	0.163	7 - 9	6s 7S	0.37	6s6p 7P*	3.46	3.09
Mo^0	379.825	0.690	7 - 9	a7S	0.00	z7P*	3.26	3.26
Mo^0	390.295	0.617	7 - 5	a7S	0.00	z7P*	3.18	3.18

The data provides two ranges of the effective electron temperature T_e. In order to explain the observed variation of T_e, first the averaging effect of the measurement must be taken into account. Namely, all spectra have been collected with a signal integration time of 2 s and averaged from five scans. Therefore, for measurements performed with HIPIMS operation frequency of 200 Hz the spectra used for T_e evaluation include up to 400 pulses. In the former study of HIPIMS discharges on Ti and Cr targets the effective electron temperature has been shown to increase at the beginning of the pulse as the electrons gain energy in electric field [8]. Afterwards a decrease of T_e is observed due to elastic and inelastic collisions with Ar and metal atoms in the pulse and afterglow phase [8]. The validity of estimated T_e values can be also confirmed taking into account the sputtering yield of Mo and W, which is of the same order as for Ti atoms [10]. Thus, the transitions in Ar take place mostly at the beginning of the pulse. As the pulse continues the electron energy is strongly decreased due to excitation and ionization of metal atoms and the electrons are thermalized below 1 eV. Since, our measurements include also the afterglow the lowest T_e of 0.2 eV can be a fingerprint of the interaction of cool electrons with the metal and Ar atoms in the afterglow phase.

Since the experiments were performed for different HIPIMS frequency it was possible to repeat the T_e calculations with respect to the frequency. Results for some of the transition lines used are depicted in Figure 4.
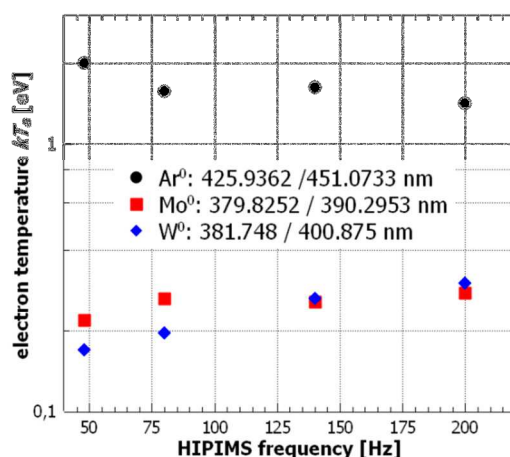
Figure 4. Frequency dependence of calculated T_e using optical emission lines of Ar, Mo and W.

Lower T_e for decreased HIPIMS frequency can be a result of a stronger influence of the transitions due to cool electrons in the afterglow phase. Since a constant signal integration time was used in all measurement the contribution of the afterglow phase for 48 Hz will be ca. four times longer compared to 200 Hz. Highest T_e estimated from Ar excitation lines is in good agreement with the literature: high energy electrons are generated at the beginning of the HIPIMS pulse and lose their energy by excitation of Ar gas [11]. As expected most of the used W and Mo excitation lines indicates T_e in the range 0.3 – 0.6 eV which is within the range of the effective electron temperature reported for Ti and Cr targets at the end of the HIPIMS pulse [8]. The most interesting is, however, the trend observed for the frequency dependence of the effective electron temperature calculated using Ar and W lines. As the frequency increases the estimated T_e decreases for Ar and increases for W. Since all parameters are kept constant except for the HIPIMS frequency this change can be a result of a decreasing refilling with Ar in the front of the target as the frequency increases.

As the plasma chemistry develops within the pulse, different species may experience a different electron temperature. The plasma density and discharge current increase gradually through the pulse. One effect of this is a concomitant severe reduction of effective electron temperature as particle collisions intensify and plasma approaches local thermal equilibrium. A second effect is the heating up and rarefaction of the gas density close to the target as a result of the increased injected power. And a third result is the gradual replacement of the gas with metal. Thus gas and metal species and their emission appear at stages of the pulse in which the effective electron temperature can be very different. As the frequency increases, power delivery rates increase due to plasma remaining from the previous pulse and amplifying the speed of development of ionisation. Due to the high mobility of electrons their temperature is likely to follow this trend and accelerate its reduction. Ion rarefaction takes place significantly slower thus reducing the effective temperature seen by Ar and increasing it for the metals.

Thus, the remaining metal atoms experience more collisions with high energy electrons. Interestingly, the T_e estimated from Ar and W emission lines are comparable for the highest HIPIMS frequency of 200 Hz. For lowest frequency the effective electron temperature calculated from Ar optical lines is higher than 2 eV but for W excitation drops down to 0.7 eV. Without further spatial and time dependent experiments the mechanism of this change and its selectivity to the observed W optical line remains unclear.

3.3. Time dependent OES measurements

The validity of the explanation could be verified by time dependent OES measurements where the line of sight of the optical fiber parallel to the target surface at a distance d=1 cm was used. The results are shown in Figure 5 for Ar^0 750 nm, Mo^0 379 nm and W^0 424 nm lines. The graph reveals a temporal evolution of optical emission from Ar and metal neutrals typical for high peak power plasma [4]. The emission from the Ar neutral is almost immediate with the increase of the current. The maximum of the Ar^0 750 nm emission line is observed after 90 μs from the pulse on. The optical emission from the Mo neutral, is delayed and starts approximately after 30 μs from the pulse on. As the Mo emission reaches its maximum shortly before the pulse off a decrease of the Ar neutral emission is observed. The same is observed for the W^0 neutral line whose intensity starts to increase even later than for the Mo^0. The maximum of the W^0 line reaches its maximum almost at the end of the pulse. In addition, as the W^0 line reaches its maximum intensity a small decrease of the Mo^0 line is observed.
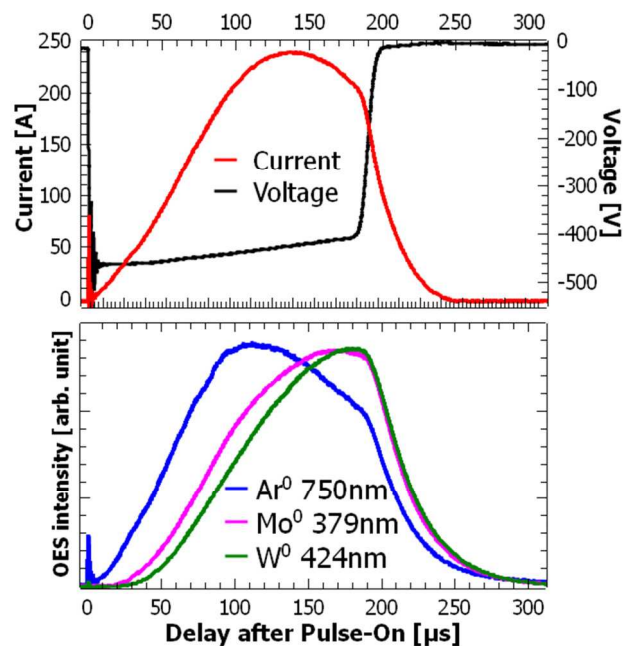

Figure 5. Temporal evolution of target current and voltage as well as the OES intensity from three dominant lines of Ar^0 (750 nm), Mo^0 (379 nm) and W^0 (424 nm). Measurements performed with f = 48 Hz, p_{Ar} = 3.2x10^{-3} mbar.

Since the measurements are performed in the vicinity of the target surface the decrease of the Ar emission can be assigned to gas rarefaction effect and a change from Ar-rich to metal-rich plasma, observed in HIPIMS discharges [4, 6, 8]. The observed change in the maximum intensity of both metal neutral lines of Mo and W suggest a complex sputtering process of both metals. The sputtering yields of Mo by Ar^+ ions normal to the surface for ion energy <1 keV are slightly higher compared to W [10]. Furthermore, the self-sputtering yields of Mo^{1+} -> Mo and W^{1+} -> W do not differ strongly [12, 13] and the sputtering yield for the tungsten carbide alloy is expected to be lower than for pure W. It can be expected that: (i) due to high ionization energy [14], low mass and low sputter yield of C atoms they do not contribute strongly to sputtering process, (ii) after the Ar gas is partially removed from the vicinity of the target, sputtering by Mo and W ions is responsible for sustaining the discharge, (iii) due to the highest atomic mass and low ionization energy tungsten will contribute to the Ar rarefaction and sputtering in the metal-rich mode.

The observed situation can be also influenced by the angular dependence of the ion emission as well as by the difference in atomic masses of C:Ar:Mo:W, which is 1 : 3 : 8 : 15. The simulations made by *Franz et al.* for HIPIMS sputtering from a LaB_2 compound target in

9

Ar atmosphere indicated a higher yield for the release of boron atoms than of lanthanum atoms upon the impact of argon (Ar -> B), boron (B -> B) and lanthanum (La -> B) [15]. The ionization energy to form Mo^{1+} and W^{1+} atoms are similar, namely, 7.09 eV and 7.86 eV, respectively. Also the ionization to Mo^{2+} and W^{2+} requires comparable amount of energy of 16.16 eV and 16.10 eV, respectively. Thus, the fraction of both metal ions can be expected to be of comparable amount. Due to spectral sensitivity restrictions of the used spectrometer the most intense W lines which are found at wavelengths below 200 nm could not be detected so even a qualitative comparison of W and Mo ions fraction cannot be made. The delay in the temporal evolution of optical emission from tungsten (Figure 5) can be an effect of independent ionization and recombination of both metals followed by different drift and diffusion influenced by differences in ion masses and ion return probability to the target. Therefore, for example spatially resolved ion energy distribution measurements are needed to provide more general model of plasma for a three-element compound target.

3.4. Gas and metal ions flux to the substrate

Figure 6 summarizes results of the flat electrostatic probe measurements. For all measurements the pulse voltage, current and length were kept constant (see Figure 1) and the average power was controlled by changing the pulsing frequency.
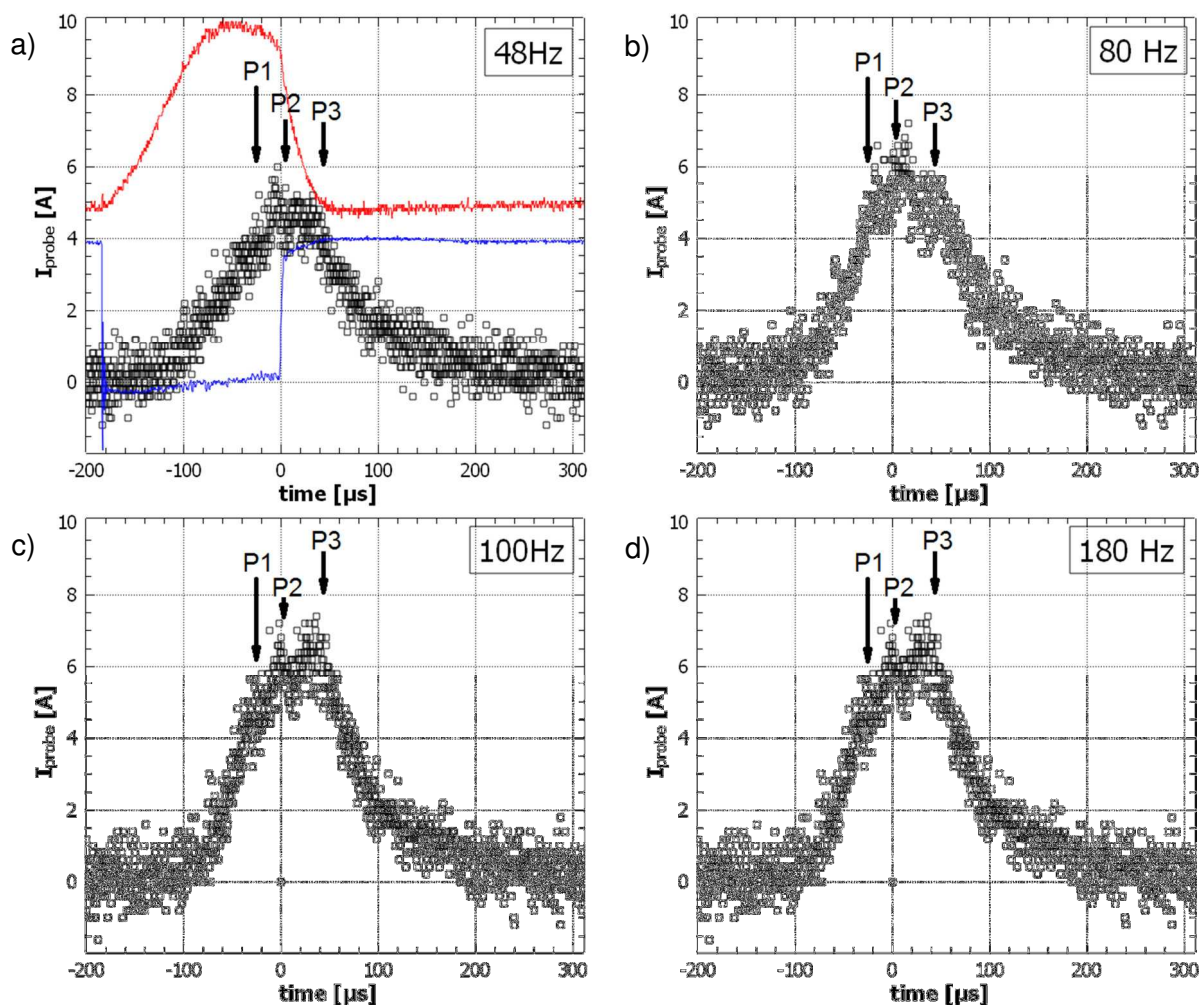

Figure 6. Temporal evolution of ion saturation current for HIPIMS discharge on Mo-W-C target in argon atmosphere ($p_{Ar} = 3.2 \times 10^{-3}$ mbar) for different HIPIMS frequency. In a) the target voltage and current in HIPIMS pulse is shown for comparison. Arrows mark the position of the ion saturation current maxima: P1 due to Ar^+ ions

first reaching the probe, P2 and P3 due to metal ions arriving at the probe at different time. See text for detailed description.

The beginning (0 μs) of the timescale was set to be equal to the end of the voltage pulse of the HIPIMS discharge as shown in Figure 6a). Therefore, the recorded probe current can be divided into two parts: (i) during the HIPIMS pulse, and (ii) in the afterglow phase.

During (i) the HIPIMS pulse the ion current follows the increase of the cathode current. The onset of the ion current is delayed 60 – 80 μs compared to the pulse beginning. This is in a reasonable agreement with the temporal evolution of the OES data (Figure 5). Several papers [4, 5, 8, 16] provided information about the temporal behavior of ion current at the substrate. It was thus concluded that gas ions generated by hot electrons first arrive at the substrate followed by the ions in the sputter wind and diffusion of bulk plasma from the target to the substrate. In some cases a third contribution to the ion current was reported due to the release of plasma when the switch off of the voltage terminates the electrostatic confinement near the target [5].

In Figure 6 the position of three peaks P1, P2 and P3 has been marked. The position and intensity of P1 and P2 depends on pulsing frequency. It is evident that, contrary to P1 and P2, the position of peak P3 does not change with HIPIMS frequency. P3 occurs 30 μs after power shut off and its intensity increases with frequency. The time-lag between successive peaks P1, P2 and P3 is in the range of 25 – 35 μs. Note, that this range of time has been also assessed for the onset of the Mo^0 emission line and the time-lag between the Mo^0 and W^0 emission lines in Figure 5.

Without extended experiments giving the insight into the dynamics of Ar, W and Mo ions only a tentative interpretation of the observed ion current can be deduced. The temporal separation of working gas and metal ions can be assumed as in the case of Ar^+ and Cr^+ ion current studied by *Greczynski and Hultman* [16]. In their experimental arrangement the Cr^+ followed the Ar^+ ions with ~30 μs delay. Similar results were obtained for Ar^+ and Ti^+ ions by *Hecimovic and Ehiasarian* who studied the temporal and spatial dependence of ion density and energy distribution [17]. The time-of-flight experiments performed by *Oks and Anders* led the authors to the same conclusions: authors pointed out the influence of sputtering yield of the metal on the composition and transport of plasma ions [18]. Therefore, the rising edge of the ion current with a small current peak marked (*P1*) in the graph can be assigned to the Ar^+ ions first reaching the probe. They are followed by metal ions *P2*, assumed to be Mo^+. The appearance of the *P3* peak would be a result of longer time-of-travel of the W ions to the probe due to their higher mass compared to Mo [14]. The time-of-travel, however, would not be influenced by the pulsing frequency itself.

A different origin of peak *P3* can be proposed by analogy to the data reported by *Breilmann et al.* [19]. For a Ti HIPIMS discharge in argon atmosphere the authors demonstrated a presence of ion current peak directly after the plasma shut off. Change in plasma potential at the end of the HIPIMS pulse which leads to a fast expansion of the sheath in front of the probe into the plasma bulk and acceleration of an increased number of ions towards the probe was proposed as the source of the peak. It is possible, that this effect does influence both peaks *P2* and *P3* which are detected within the first 20 μs after the HIPIMS pulse is off. The fact, that *P3* is detected in all cases at the same time after the pulse off supports a constant travel time of one type of ions.
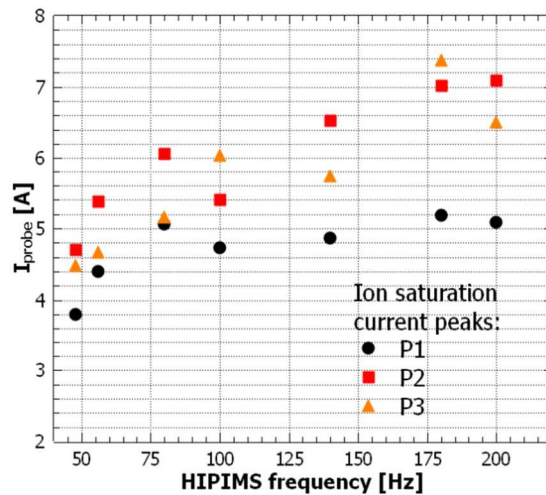
Figure 7. The frequency dependence for three maxima of the ion saturation current measured for Mo-W-C target in argon atmosphere.

As shown in Figure 7 the increase of the ion current with frequency is faster for peaks *P2* and *P3*. Since the discharge parameters are kept constant this can be explained by an increase of the total density of ions with the increase of the average power.

Indeed, the frequency dependent optical emission spectra shown in Figure 8 indicates a remarkable increase of metal line intensities with the increase of HIPIMS frequency.
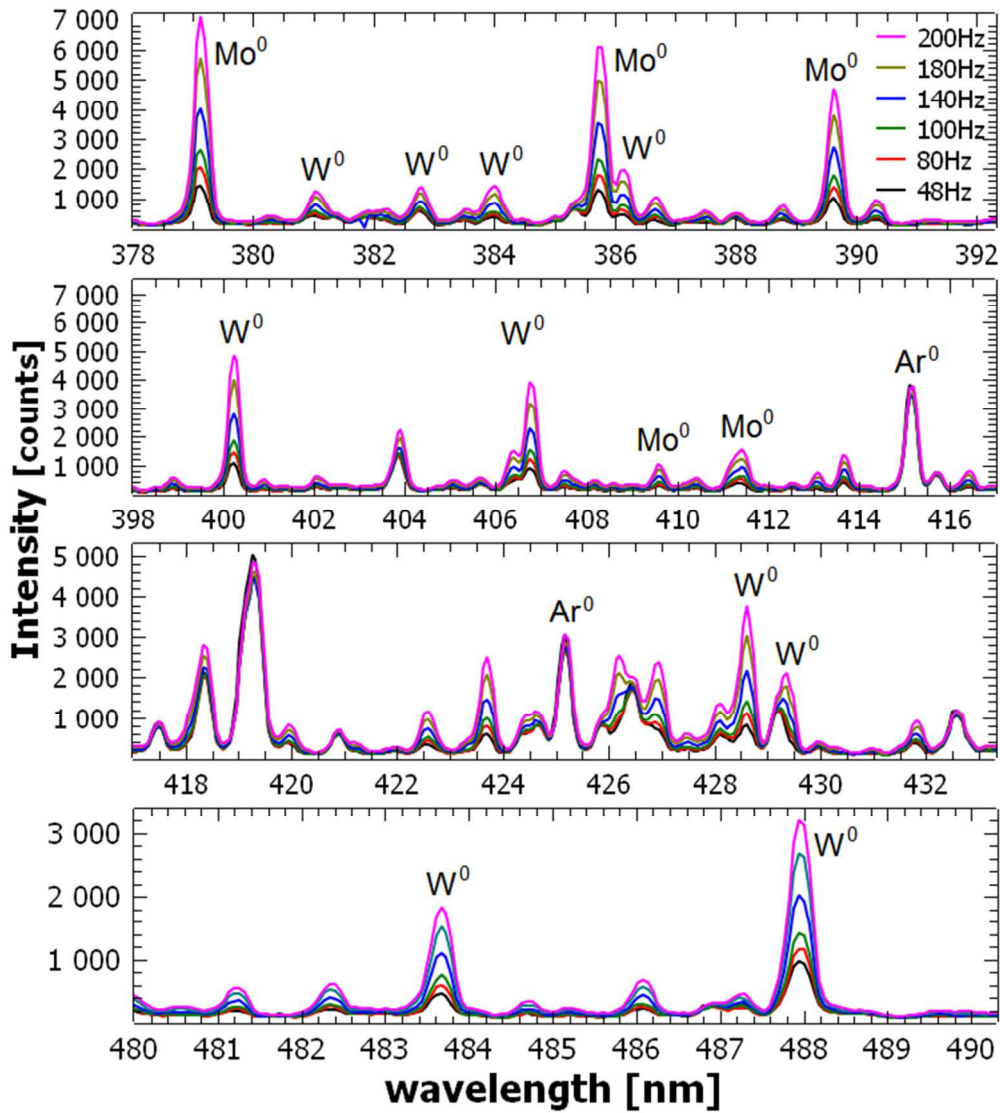
Figure 8. Frequency dependence of the optical emission spectrum of high power impulse sputtering of Mo-W-C in an argon atmosphere ($p_{Ar} = 3.2 \times 10^{-3}$ mbar).

Note, that each spectra was measured with integration time of 2 seconds and averaged five times. Therefore, the change of the HIPIMS frequency changes the number of pulses included in the measurement window. To eliminate this effect the intensities of metal lines were compared as a ratio to two Ar neutral lines as summarized in Figure 9.
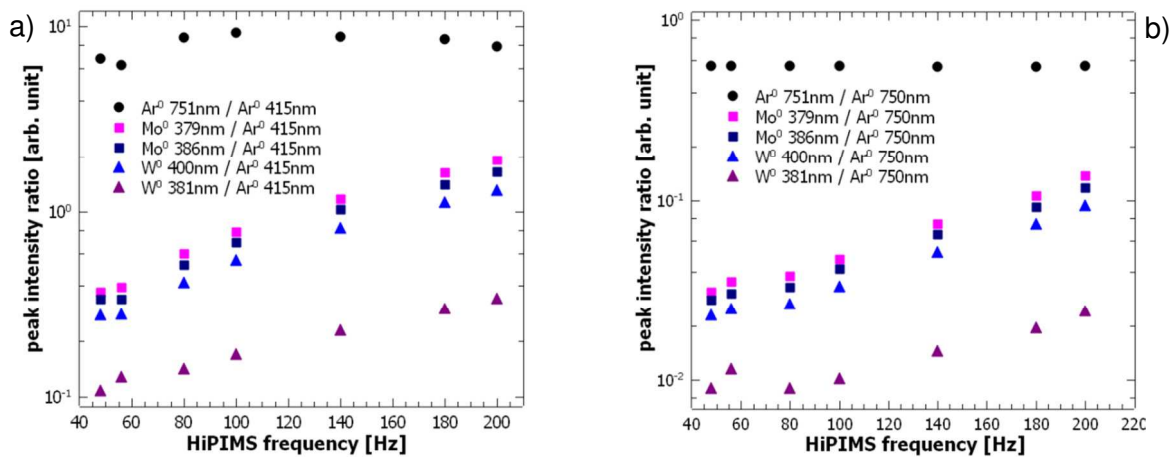
Figure 9. Frequency evolution of the intensity ratio of dominating metal and argon optical emission lines measured in HIPIMS discharge in argon atmosphere. In a) the ratio of the metal lines to the Ar^0 415.859 nm and in b) the ratio of metal lines to the Ar^0 750.387 nm have been shown, respectively.

As the graph reveals, the ratio of the Ar neutral lines 751.460 nm to 750.387 nm does not change with the frequency and the ratio of Ar 751.460 nm to 415.859 nm Ar neutral line shows only small fluctuation with the HIPIMS pulse frequency. In contrast, the ratio of W and Mo intensities to Ar^0 750.387 nm and Ar^0 415.859 nm increases with frequency. Additionally, the increase is not linear and it is faster for HIPIMS frequencies higher than 100 Hz.

Since the line intensity is related to the density of species in the plasma the data confirms an increase of metal metastables and ion density with the increase of HIPIMS frequency. This supports also the measurements of the ion current where an increase of ion current with increase of frequency was observed.

4. Conclusions

This work comprises an indepth study of a HIPIMS discharge on a multicomponent target of Mo-W-C operated in argon atmosphere.

Optical emission spectroscopy measurements allowed to identify the majority of metal and gas lines in the wavelength range 300-800 nm. The effective electron temperature was estimated based on the OES data. In agreement with literature, a higher T_e was found at the beginning of the HIPIMS pulse where the interaction of electrons with argon is dominant. In the later part of the pulse the presence of thermalized electrons interacting with metal atoms was concluded.

These data were confirmed by time-resolved OES measurements, which showed the Ar emission to be almost immediate with the increase of HIPIMS pulse current. It was followed by Mo and W emission with 30 µs and 50 µs delay, respectively. The temporal dependence of the OES signal confirmed Ar gas rarefaction at the end of the HIPIMS pulse. Influence of working gas and target metal ions was proposed to explain the temporal dependence of the ion saturation current.

Finally, an increase in the metal content in the plasma with frequency has been demonstrated to occur in conjunction with an increase in ion saturation current.

To our knowledge, this is a first report on the temporal and spatial dependence of ion flux from a two- component target. Our data show the possibility to influence the metal ion concentration and flux by the change of HIPIMS frequency, thus the possibility to enhance the adhesion and to modify the hardness of the deposited film as discussed by *Madal et al.* [2]. Further experiments including ion mass spectroscopy are, however, necessary to explain all issues related to the frequency dependence of ion current to the substrate.

References

[1]   Q. Wei, R. Narayan, A. Sharma, J. Sankar and J. Nara, „Preparation and mechanical properties of composite diamond-like carbon thin films," *J. Vac. Sci. Technol. A,* 17 (2009) 3406.

[2]   P. Mandal, A. Ehiasarian and P. Hovsepian, „Tribological behaviour of Mo–W doped carbon-based coating at ambient condition," *Tribol. Int.,* 90 (2015) 135-147.

[3]   A. Voevodin, S. Prasad and J. Zabinski, „Nanocrystalline carbide/amorphous carbon

composites," *J. Appl. Phys.,* 82 (1997) 855.

[4] A. Ehiasarian, R. New, W. Muenz, L. Hultman, U. Helmersson and V. Kouznetsov, „Influence of high power densities on the composition of pulsed magnetron plasmas," *Vacuum,* 65 (2002) 147–154.

[5] A. Hecimovic, K. Burcalova and A. Ehiasarian, „Origins of ion energy distribution function (IEDF) in high power impulse magnetron sputtering (HIPIMS) plasma discharge," *J. Phys. D: Appl. Phys.,* 41 (2008) 095203.

[6] A. Anders, „Discharge Physics of High Power Impulse Magnetron Sputtering," *Surface & Coatings Technology,* 205 (2011) S1–S9.

[7] H. R. Griem, Principles of Plasma Spectroscopy, Cambridge University Press, 1997.

[8] A. Vetushka and A. Ehiasarian, „Plasma dynamic in chromium and titanium HIPIMS discharges," *J. Phys. D: Appl. Phys.,* 41 (2006) 015204.

[9] NIST (National Institute of standards and technology) atomic spectra database, 2016 [Online]. Available: http://physics.nist.gov/PhysRefData/ASD/lines_form.html.

[10] N. Matsunami, Y. Yamamura, Y. Itikawa, N. Itoh, Y. Kazumata, S. Miyagawa, K. Morita, R. Shimizu and H. Tawara, „Atomic Data," *Nuclear Data Tables,* 31 (1984) 1.

[11] J. Gudmundsson, N. Brenning, D. Lundin and U. Helmersson, „High power impulse magnetron sputtering discharge," *Journal of Vacuum Science & Technology. A.Vacuum, Surfaces, and Films,* 30 (2012) 030801.

[12] C. Garcla-Rosales, W. Eckstein and J. Roth, „Revised formulae for sputtering data," *J. Nucl. Mater.,* 218 (1994) 8-17.

[13] E. Salonen, T. Jarvi, K. Nordlund and J. Keinonen, „Effects of the surface structure and cluster bombardment on the self-sputtering of molybdenum," *J. Phys.: Condens. Matter,* 15 (2003) 5845–5855.

[14] A. Anders, J. Andersson and A. Ehiasarian, „High power impulse magnetron sputtering: Current-voltage-time characteristics indicate the onset of sustained self-sputtering," *J. Appl. Phys.,* 102 (2007) 113303.

[15] R. Franz, C. Clavero, R. Bolat, R. Mendelsberg and A. Anders, „Observation of multiple charge states and high ion energies in high power impulse magnetron sputtering (HiPIMS) and burst-HiPIMS using a LaB6 target," *Plasma Sources Science and Technology,* 23 (2014) 035001.

[16] G. Greczynski and L. Hultman, „Time and energy resolved ion mass spectroscopy studies of the ion flux during high power pulsed magnetron sputtering of Cr in Ar and Ar/N2 atmospheres," *Vacuum,* 84 (2010) 1159-1170.

[17] A. Hecimovic and A. Ehiasarian, „Spatial and temporal evolution of ion energies in high power impulse magnetron sputtering plasma discharge," *Journal of Applied Physics,* 108 (2010) 063301.

[18] E. Oks and A. Anders, „Evolution of the plasma composition of a high power impulse magnetron sputtering system studied with a time-of-flight spectrometer," *Journal of Applied Physics,* 105 (2009) 093304.

[19] W. Breilmann, C. Maszl, J. Benedikt and A. von Keudell, „Dynamic of the growth flux at the substrate during high-power pulsed magnetron sputtering (HiPIMS) of titanium," *J. Phys. D: Appl. Phys.,* 46, (2013) 485204.